Heat and Mass Transfer of Rectangular Waveform Inflow Impinging Synthetic Jet at Same Strouhal Number

Xin Yue Huang, Ping Li*

MOE Key Laboratory of Thermal Fluid Science and Engineering, Xi'an Jiaotong University, Xi'an, Shaanxi Province, 710049, P. R. China
pingli@xjtu.edu.cn

Heat removal capacity of slot synthetic jet impinging on target plate with constant heat flux is numerically studied in this work. The signal of synthetic jet velocity is rectangular waveform; parameters investigated cover dimensionless jet-to-surface distance H/w=2 and 4, Reynolds number Re 10,000 – 20,000, oscillating frequency f 10 Hz – 20 Hz, and corresponding Strouhal number St of 0.1598. The results indicated that heat transfer rate of synthetic jet at H/w=4 is higher than that at H/w=2 with other conditions unchanged, which is attributed to the discrepancy between flow structures. The extent of Nusselt number Nu enhancement as a result of Re promotion, increases with H/w. Moreover, under the circumstance of rectangular waveform and identical H/w, the similarity of area-averaged Nusselt number <Nu> variation process emerges under the same St that roots in the comparability of flow field evolution.

1. Introduction

Impingement jet is a promising cooling method that is widely used in industrial applications (Kajitani et al., 2019) as a result of its high localized heat transfer rate. Compared to the conventional one, synthetic jet (Glezer and Amitay, 2002) that introduces fluid carried with adequate momentum without net mass transfer, has attracted more attention.

There are extensive studies concerning the factors on impinging heat transfer characteristics of synthetic jet. Among them, the jet-to-plate spacing and Strouhal number St, or the stroke length, are two notable parameters. The experimental study conducted by Ghaffari et al. (2016) suggested that there is a degradation for heat transfer as the jet-to-plate spacing shortens. Similarly, Greco et al. (2018) indicated that time-averaged stagnation Nusselt number increases with the spacing. Whereas the consistent conclusion arrives from foregoing studies, the larger spacing does not blindly lead to better heat performance, as an optimum jet-to-plate spacing, but not the largest, within the studied range was proposed by Gillespie et al. (2006). Furthermore, Pavlova and Amitay (2006) pointed out that the optimum spacing is highly reliant on stroke length. Valiorgue et al. (2009) showed that the functional form of stagnation Nusselt number depends on which range the stroke length is in. That is to say, the effects of the two parameters cannot be considered in isolation.

Greater emphasis has been placed on synthetic jet with sinusoidal velocity waveform in previous studies. Nevertheless, there are other feasible shapes of unsteadiness for impingement synthetic jet cooling, such as triangular, rectangular waveform (Herwig and Middelberg, 2008) and other composite ones (Geng et al., 2015); from the literature review, the research deficiency exists on heat and mass transfer process of the synthetic jet in other velocity waveforms.

In the present study, the heat and mass transfer of synthetic jet cooling is numerically analyzed. More specifically, the impacts of jet-to-plate spacing H and St on heat removal capacity for synthetic jet with rectangular velocity waveform have been discussed in detail.

2. Methods

2.1 Physical model

The two-dimensional symmetric physical model that is the same as the previous work (Li et al. 2019), is adopted to study the confined impingement slot synthetic jet. Figure 1 depicts the model sketch. Likewise, the jet orifice width w and the target surface length L are 6 mm and 120 mm; the heated part with a length of 60 mm lies in the middle of impingement plate. The dimensionless nozzle-to-plate distance H/w, i.e. the ratio of nozzle-to-plate distance H to jet orifice width w, is 2 and 4. The letters x and y denote the coordinate parallel to plate and normal to plate, respectively.
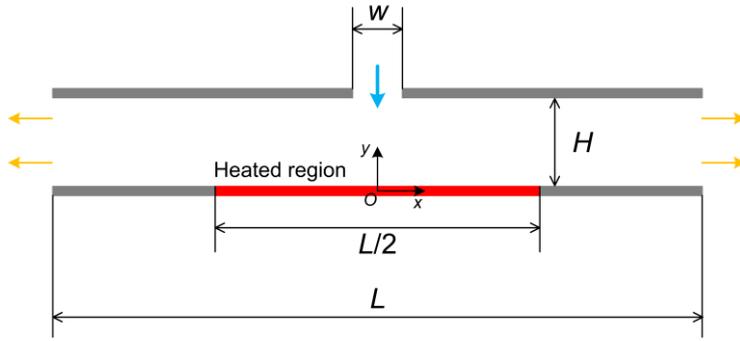
Figure 1: Physical model sketch

The working medium is water at 298.15 K, 101,325 Pa. Inlet velocity u(t) is in rectangular waveform with the duty cycle of 0.5. The incident direction of synthetic jet is perpendicular to the inlet. The opening boundary with averaged pressure of 101,325 Pa is specified at the outlet. Impingement plate is set as no-slip wall while heated region providing a uniform heat flux q of 1,000,000 W·m^{-2}. The rest parts, which are painted gray in Figure 1, are all regarded as no-slip and adiabatic walls.

2.2 Governing equations

The whole process of heat and mass transfer in the present study is regarded as unsteady, incompressible and turbulent, while physical properties of working fluid remain invariant.
The shear stress transport k-ω (SST/k-ω) model is adopted. The governing equations are written as follows considering the above assumptions:

$$\frac{\partial \overline{u_i}}{\partial x_i} = 0 \tag{1}$$

$$\rho \left(\frac{\partial \overline{u_i}}{\partial t} + \frac{\partial \overline{u_i u_j}}{\partial x_j} \right) = -\frac{\partial \overline{p}}{\partial x_i} + \frac{\partial}{\partial x_i} \left[\mu \left(\frac{\partial \overline{u_i}}{\partial x_j} + \frac{\partial \overline{u_j}}{\partial x_i} \right) - \rho \overline{u_i' u_j'} \right] \tag{2}$$

$$\frac{\partial T}{\partial t} + u_j \frac{\partial T}{\partial x_j} = \alpha \frac{\partial}{\partial x_j} \frac{\partial T}{\partial x_j} - \frac{\partial \overline{u_j' T'}}{\partial x_j} \tag{3}$$

where the term of $-\rho \overline{u_i' u_j'}$ represents the Reynolds stresses; T merely symbolizes the temperature only when appearing in governing equations; ρ denotes water density; μ refers to dynamic viscosity coefficient of water; α is the thermal diffusivity of water; t signals the time. The governing equations are solved via ANSYS CFX.
The Boussinesq assumption is presented as:

$$-\rho \overline{u_i' u_j'} = \mu_t \frac{\partial \overline{u_i}}{\partial x_j} \tag{4}$$

where μ_t is the eddy viscosity (Launder and Sandham, 2002):

$$\mu_t = \frac{a_1 k}{\max(a_1 \omega, SF_2)} \tag{5}$$

where k stands for the turbulence kinetic energy, ω for the specific dissipation rate; the specific value for a_1 is 0.31 while the F_2 is equal to 0 in the boundary layer and 1 in free shear layer flow.

Governing equations are discretized based on the finite volume method. The convective term is solved by high resolution scheme as the transient term by second-order backward Euler scheme.

Inlet velocity u(t) is given in Eq(6), where f denotes the oscillating frequency:

$$u(t) = 2U_0 \frac{\tanh[K \sin(2\pi f t)]}{\tanh(K)} \tag{6}$$

where the value of K is 10,000; U_0 will be discussed later in the Section 2.3.

2.3 Calculation of non-dimensional parameters

Reynolds number is defined as the following Eq(7):

$$Re = \frac{\rho U_0 D}{\mu} \tag{7}$$

where D represents the slot hydraulic diameter equal to 2w; U_0 denotes the averaged velocity:

$$U_0 = \frac{1}{T} \cdot \int_0^{T/2} u(t)dt \tag{8}$$

where T signals the period length.

Basic form of Nusselt number is given in Eq(9):

$$Nu(x,t) = \frac{hD}{\lambda} = \frac{q}{T_w(x,t) - T_\infty} \cdot \frac{2w}{\lambda} \tag{9}$$

where $T_w(x,t)$ and T_∞ signal local instantaneous temperature on target surface as well as ambient temperature, respectively; λ denotes thermal conductivity of water; h stands for convective heat transfer coefficient.

Time-area averaged Nusselt number Nu_{avg}, is defined in Eq(10):

$$Nu_{avg} = \frac{1}{\Delta t} \frac{1}{\Delta x} \int_0^T \int_0^{L/2} Nu(x,t)dxdt \tag{10}$$

Moreover, area-averaged Nusselt number <Nu> is given in Eq(11):

$$\langle Nu \rangle = \frac{1}{\Delta x} \int_0^{L/2} Nu(x,t)dx \tag{11}$$

Math expression of Strouhal number is given in Eq(12):

$$St = \frac{fD}{U_0} \tag{12}$$

2.4 Grid/ time step independence study and validation of numerical scheme

Considering the demands of SST/k-ω turbulence model, the first layer of grid near the plate satisfies the requirements of dimensionless distance from the wall $y^+ \approx 1$. The grid independence study is conducted among four sets of grids under the condition of f=20 Hz, Re=20,000, H/w=4; time-area averaged temperature at the heated target wall T_{wall} serves as the indictor. Sizes of the four sets of grids are enumerated as follows: x×y=270×60 for Grid 1, x×y=300×70 for Grid 2, x×y=340×80 for Grid 3 and x×y=370×90 for Grid 4. Relative deviation of T_{wall} for other sets from Grid 3 is not more than the threshold 5%. Grid 3 is adopted for further study, taking into account both accuracy and efficiency.

Four kinds of dimensionless time step length (t_Δ signals practical time step length), t_Δ/T=0.04, 0.02, 0.01 and 0.005, are investigated in time step independence study; t_Δ/T=0.01 is chosen after evaluating relative deviation. The numerical scheme validation is conducted through comparing results based upon current numerical scheme and experimental outcomes of Gardon and Akfirat (1966), under the same condition of Re=11,000, H/w=6. The

numerical results are well-fitted to experimental ones; therefore, the proposed numerical model is confirmed effective for subsequent analysis.

3. Results and discussion

Figure 2 elucidates the overall heat transfer rate represented by time-area averaged Nusselt number Nu_{avg} for groups with various H/w, each of which involves three different cases for Re and f.
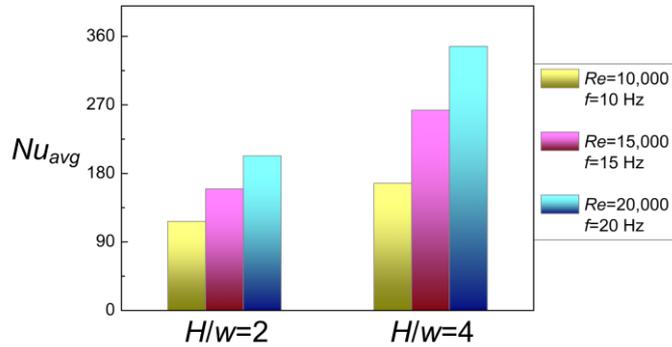
Figure 2: Nu_{avg} of various conditions classified by H/w

From Figure 2, the maximum Nu_{avg} is achieved at Re=20,000 f=20 Hz H/w=4 while the minimum at Re=10,000 f=10 Hz H/w=2. Moreover, evidently from Figure 2, Nu_{avg} for H/w=4 is higher than that for H/w=2 at the same Re and f. Furthermore, seemingly paradoxically, heat transfer rate for Re=15,000 f=15 Hz H/w=4 surpasses the one for Re=20,000 f=20 Hz H/w=2. To illustrate this phenomenon, Figure 3 depicts how flow field transforms within one period roughly via describing that at four critical moments. The two selected calculation conditions would account for foregoing results in Figure 2 to some extent. As for the case of Re=15,000 f=15 Hz H/w=4, a considerable primary vortex has always been located above the heated region throughout the whole period. At 0.49T, at which the fluid with relatively high momentum reaches nearby the heated region, the primary vortex squeezes the fluid resulting in spread of high velocity fluid above the heated region. By contrast, the vortex for the case of Re=20,000 f=20 Hz H/w=2 that is smaller in scale in comparison with former case, is more powerless in squeezing the high momentum fluid near the heated target wall. In spite of larger averaged speed of synthetic jet at higher Re, a portion of high velocity fluid flees away from the target wall, and therefore heat removal has not been effectively enhanced.
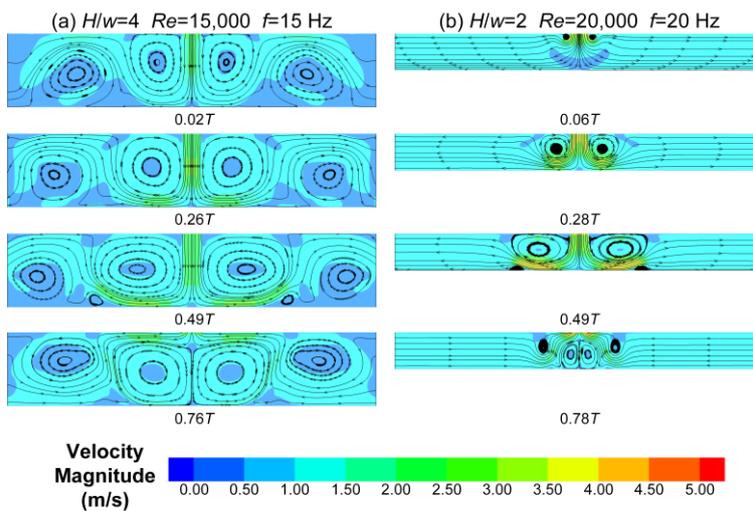
Figure 3: Velocity contour and streamline at four critical normalized moments for H/w=4 Re=15,000 f=15 Hz and H/w=2 Re=20,000 f=20 Hz

Figure 4 illustrates how the area averaged Nusselt number <Nu> varies within two successive periods under different Re or f grouped by H/w. As indicated in the previous study (Li et al. 2020), variation curves for <Nu> with normalized time are analogous in two cases at the same St but with disparate Re or f. In present study, more factors such as geometrical parameters, i.e. H/w=2 and 4, as well as rectangular waveform have been supplemented. As demonstrated in Figure 4, the similarity also emerges in the conditions of rectangular waveform, H/w=2 or 4, St=0.1598. Additionally, it should also be noted that differences of <Nu> between various Re or f cases fluctuate with H/w. Specifically, the increase of <Nu> from the case Re=10,000 f=10 Hz (or Re=15,000 f=15 Hz) to Re=15,000 f=15 Hz (or Re=20,000 f=20 Hz), reduces as H/w falls from 4 to 2. From Figure 4, the gaps of <Nu> variation curves between different conditions, is obviously compressed at H/w=2, which is also supported by Figure 2.
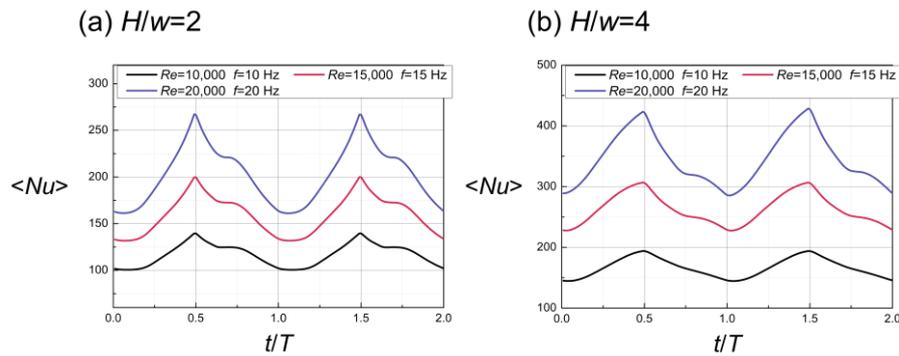
Figure 4: <Nu> variations with t/T in two successive periods under different Re or f grouped by H/w

To find out the causes behind this similarity, Figure 5 depicts the corresponding flow fields for Re=10,000 f=10 Hz and Re=20,000 f=20 Hz respectively at H/w=2 and 4.
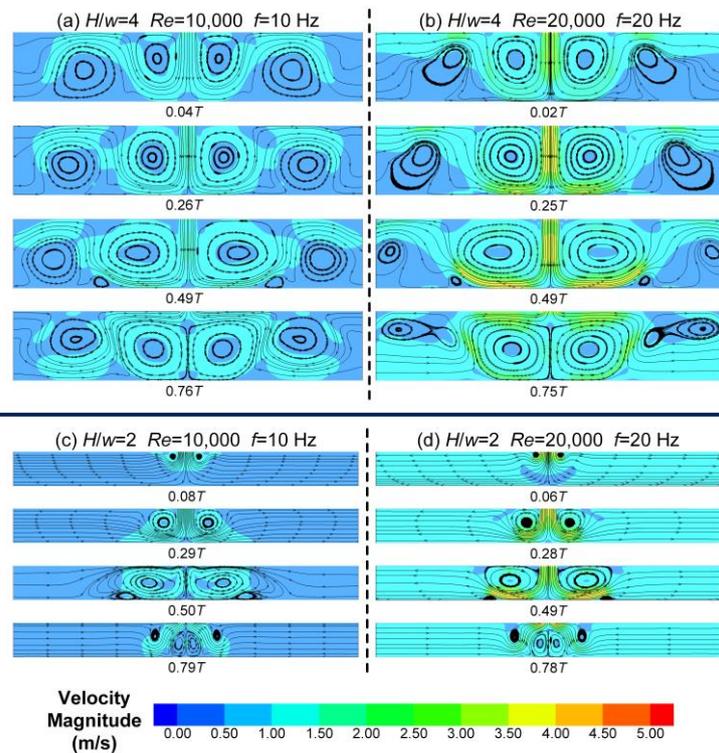
Figure 5: Velocity contour and streamline at four critical normalized moments for Re=10,000 f=10 Hz and Re=20,000 f=20 Hz classified by H/w

From Figure 5, in the situation of H/w=4, evolving process of the primary vortex resembles each other. The same rule is tenable for the case of H/w=2. It should also be noted that because of the characteristics of rectangular waveform, the primary vortex behaves variously at several corresponding moments, e.g. 0.50T for H/w=2 Re=10,000 f=10 Hz and 0.49T for H/w=2 Re=20,000 f=20 Hz, nevertheless, flow field evolution processes of the same St and H/w are similar on the whole.

4. Conclusions

The heat and mass transfer process of synthetic jet impingement cooling is numerically studied in present work. The main conclusions are as follows:

(1) For the same Re and f, the heat removal capacity of rectangular synthetic jet at H/w=4 is greater than that at H/w=2; in the case of Re=15,000 f=15 Hz H/w=4, Nu_{avg} even surpasses that for Re=20,000 f=20 Hz H/w=2. This phenomenon roots in the discrepancy of flow structures, especially the evolution of primary vortex above heated target wall, as well as triggering consequence.

(2) Under the circumstance of rectangular waveform and uniform H/w, the similarity of <Nu> evolution emerges under the same St. Furthermore, in the condition of the same St, the extent of Nu enhancement as a result of Re promotion, increases with H/w.

(3) In cases of rectangular waveform, at identical H/w, the similarity of flow field evolution leads to that of heat transfer process in the condition of the same St.

Acknowledgements

References

Gardon R., Akfirat J.C., 1966, Heat transfer characteristics of impinging two-dimensional air jets, ASME Journal of Heat Transfer, 88(1), 101–107.

Geng L., Zheng C., Zhou J., 2015, Heat transfer characteristics of impinging jets: The influence of unsteadiness with different waveforms, International Communications in Heat and Mass Transfer, 66, 105–113.

Ghaffari O., Solovitz S.A., Arik M., 2016, An investigation into flow and heat transfer for a slot impinging synthetic jet, International Journal of Heat and Mass Transfer, 100, 634–645.

Gillespie M.B., Black W.Z., Rinehart C., Glezer A., 2006, Local convective heat transfer from a constant heat flux flat plate cooled by synthetic air jets, ASME Journal of Heat Transfer, 128, 990–1000.

Glezer A., Amitay M., 2002, Synthetic jets, Annual Review of Fluid Mechanics, 34, 503–529.

Greco C.S., Paolillo G., Ianiro A., Cardone G., de Luca L., 2018, Effects of the stroke length and nozzle-to-plate distance on synthetic jet impingement heat transfer, International Journal of Heat and Mass Transfer, 117, 1019–1031.

Herwig H., Middelberg G., 2008, The physics of unsteady jet impingement and its heat transfer performance, Acta Mechanica, 201, 171–184.

Kajitani R., Mukaida T., Kataoka K., Ohmura N., 2019, Characteristics of a falling liquid flow using periodic jetting flow, Chemical Engineering Transactions, 74, 991–996.

Launder B.E., Sandham N.D., 2002, Closure strategies for turbulent and transitional flows, Cambridge University Press, Cambridge, UK, DOI:10.1017/CBO9780511755385.

Li P., Guo D., Liu R., 2019, Mechanism analysis of heat transfer and flow structure of periodic pulsating nanofluids slot-jet impingement with different waveforms, Applied Thermal Engineering, 152, 937–945.

Li P., Huang X., Guo D., 2020, Numerical analysis of dominant parameters in synthetic impinging jet heat transfer process, International Journal of Heat and Mass Transfer, 150, 119280.

Pavlova A., Amitay M., 2006, Electronic cooling using synthetic jet impingement, ASME Journal of Heat Transfer, 128, 897–907.

Valiorgue P., Persoons T., McGuinn A., Murray D.B., 2009, Heat transfer mechanisms in an impinging synthetic jet for a small jet-to-surface spacing, Experimenal Thermal and Fluid Science, 33, 597–603.